PHYSICAL REVIEW B **84**, 235143 (2011)

Dilution effect on the U 5f states in Au matrix: A photoemission spectroscopy study

R. Eloirdi,[*] T. Gouder, F. Wastin, and F. Huber
European Commission, Joint Research Centre, Institute for Transuranium Elements, Postfach 2340, D-76125 Karlsruhe, Germany

A. B. Shick
European Commission, Joint Research Centre, Institute for Transuranium Elements, Postfach 2340, D-76125 Karlsruhe, Germany and Institute of Physics, Academy of Sciences of the Czech Republic, Na Slovance 2, CZ-182 21 Prague, Czech Republic

J. Kolorenč
Institute of Physics, Academy of Sciences of the Czech Republic, Na Slovance 2, CZ-182 21 Prague, Czech Republic

(Received 24 September 2011; revised manuscript received 2 December 2011; published 27 December 2011)

U_xAu_{100-x} thin films ($x = 0$ to 100 at.%) have been prepared by sputter deposition and studied *in situ* by use of x-ray photoemission spectroscopy and ultraviolet spectroscopy. The valence band displays a two-peak structure near the Fermi level (E_F), one (peak α) pointing at E_F, characteristic of itinerant 5f states, and one (peak β) at ~0.7 eV, which is representative of localized 5f states. The presence of the peak α at all the composition of the series ($x = 0$ to 100 at.%) shows that 5f states are never purely localized. The evolution of the full width at half maximum of the 5f line displays three main domains of composition where the interaction evolves from a (5f, ligand states) ($x < 25$ at.%) hybrid band to a pure 5f band ($x > 50$ at.%). In an intermediate domain (30–50 at.%), the Au 5d6s conduction band narrows and shifts to higher binding energy at the extent of the interaction with U 5f states. A correlation of the valence band spectra is made with the U 4f core-level peak where the shape evolves from a three-peak structure ($x < 10$ at.%), characteristic of a mixed valence state, to a single-peak structure ($x \geqslant 30$ at.%). Relativistic electronic structure theory based on the local density approximation plus exact diagonalization of a multiorbital Anderson impurity model explains well the valence photoemission features. The essential role of hybridization in the U-based systems is emphasized.

DOI: 10.1103/PhysRevB.84.235143 PACS number(s): 71.20.Gj, 71.28.+d

I. INTRODUCTION

In this study, we investigate the evolution of the electronic structure of uranium and, in particular, the localization of the 5f states, as uranium is diluted in a gold matrix. The dilution of uranium atoms in gold matrix may lead to two contrary effects. On the one hand, the direct 5f-5f overlap of neighboring U atoms is suppressed and, above a critical distance (Hill limit: 0.34–0.36 nm), the 5f may tend to be localized if hybridization to Au states is weak. On the other hand, bonding between U and Au atoms favors hybridization between U 5f and Au 5d states, giving rise to the formation of a hybrid band, thus leading to itinerant 5f states.

The present study on the U_xAu_{100-x} system is based on the following series of experiments conducted on U_xRh_{100-x},[1] U_xPd_{100-x},[2] and U_xAg_{100-x}[3] thin films. In rhodium and palladium, the 4d band is an incomplete shell and, thus, pinned at the Fermi level. This enables overlapping with the 5f states, leading to the formation of intermetallic system UM (M = Rh, Pd). In a rhodium matrix, the 5f states are always delocalized independently of the uranium concentration. In palladium they undergo a localization at the composition of $U_{25}Pd_{75}$ where also UPd_3 intermetallic has localized 5f states. For higher dilution, the 5f states stay localized. In silver, the d band is filled and Ag does not bond with uranium. The 5f are delocalized down to 5 at.% of uranium. Whereas in the gold matrix, despite an almost-filled Au 5d band (similarly to Ag 4d), gold forms a bond with uranium as demonstrated by its two stable compounds[4] (similarly to Rh and Pd). This dual character allows us to investigate how the localization of the 5f states can be affected.

The phase diagram of the U-Au system[4] shows two stable compounds at room temperature: $U_{14}Au_{51}$, initially reported as "UAu_3," and UAu_2.[5] $U_{14}Au_{51}$ is a moderately heavy fermion ($\gamma = 300$ mJ K^2/mol U),[6] showing a state intermediate between localized and itinerant states. The solubility of U in Au is low, below 1%. However, a statistical mixture of U and Au atoms far from the thermodynamic equilibrium can be obtained by sputter deposition. The large quenching rate of the technique allows off-stoichiometric films to be prepared.

Since "impurity" atoms, whose atomic levels (f) interact with the conduction band of the ligand atoms, play an important role in the onset of heavy-fermion (HF) property, investigating such systems in a wide concentration range would allow us to follow and observe the onset of the heavy-fermion behavior via the correlation effects in photoemission. Thus, U_xAu_{100-x} films were produced by use of a codeposition technique, which allows us to prepare all intermediate compositions from a pure Au film ($x = 0$ at.%) to a pure U film ($x = 100$ at.%).

Moreover, contradictory results on the nature of the 5f states in the compound "UAu_3" have been reported in the literature. While Schneider *et al.*[7] report itinerant 5f states, Petit *et al.*[8] conclude, in a theoretical work, a 5f^2 localized state similar to that in UPd_3. For highly diluted U in a Au matrix very few studies[9,10] have been reported. They indicate a multipeak structure for U 4f while no signal peak was observed at E_F. By use of ultraviolet spectroscopy (UPS) and x-ray photoemission spectroscopy (XPS) on the series of U_xAu_{100-x} thin films, we intend to shed light on this controversy.

This paper is organized as follows: In Secs. II and III we describe the experimental techniques and the experimental results for valence and core-level photoemission in the U_xAu_{100-x} films. In Sec. IV we present the results of the electronic structure calculations based on static and dynamical mean-field theories. These results are compared with available experimental data.

II. EXPERIMENTAL

The U_xAu_{100-x} films were prepared by use of sputter codeposition from elemental U and Au targets. A wide concentration range ($x = 0$ to 100 at.%) was covered by adjusting the respective sputter rates of the two targets by varying the respective voltages (−100 to −1000 V). Syntheses were performed under an ultra-high-purity (99.9999%) Ar atmosphere at a pressure of 0.67 Pa. The targets were a U metal disk (99.9% purity, 5-mm radius, 1-mm thickness) and a Au wire loop (99.9%) placed 1 mm below the U target, both kept at at room temperature by air cooling. The plasma in the diode source was maintained by injecting electrons of 50- to 100-eV kinetic energy. Shields were installed to expose only the sample to the Ar-U-Au plasma and keep the contamination of the chamber as low as possible. The deposition rates were about 0.1 nm s^{-1}. Photoemission measurements were done on films of about 20-nm thickness, deposited at room temperature on a Si(111) wafer. The background pressure in the plasma chamber was 1.33×10^{-7} Pa. Photoemission data were recorded *in situ* using a Leybold LHS-10 hemispherical analyzer. XPS spectra were taken using MgKα (1253.6-eV) radiation with an approximate resolution of 0.9 eV. UPS measurements were made using He I and He II (21.22- and 40.81-eV) excitation radiation, produced by a windowless UV rare gas discharge source. The total resolution in UPS was 0.1 to 0.05 eV for the high-resolution scans. All measurements were conducted in a UHV spectrometer at an operating pressure of 2.6×10^{-8} Pa.

III. RESULTS AND DISCUSSION

A. Valence band study

The evolution of the He II valence band spectra of a series of U_xAu_{100-x} films ($x = 0$ to 100 at.%) is reported in Fig. 1 and compared to Au and U films as references.

The valence band spectrum of the Au film consists of a plateau corresponding to an *sp* conduction band (0–2 eV) and of the Au 5*d* band, 6 eV wide, centered at about 5 eV below E_F. This is in agreement with spectra observed for bulk Au.[11,12] Because the Au 5*d* band is almost filled (5*d* levels stabilized by $5d^{10}6s^1 \leftrightarrow 5d^96s^2$ rehybridization),[13,14] it is located well below E_F. The pseudogap between peak A and peak B of Au 5*d* [Fig. 1(a)] reflects the spin-orbit splitting. Adding U has, in principle, two effects on the Au 5*d* band, a narrowing and a shift. These two features are related to the alteration of the atomic environment of Au and to a charge redistribution. Initially, adding uranium ($x \leqslant 10$ at.%) induces a small shift of the Au 5*d* band toward E_F. This is an indication that Au 5*d* may be depleted, relative to Au metal.

The U states are mainly located between E_F and 2 eV BE. Because of the small energy overlap with the Au 5*d* states, there is only a weak bonding between the Au 5*d* and the U 6*d*5*f* states. The weak bonding between U and Au is indeed demonstrated by a higher oxidation rate of U-Au compounds, when compared to U-Pt compounds.[7] The shape of the 5*f* emission strongly depends on the film composition [Fig. 1(b)]. The two features, labeled α and β, are attributed to 5*f* states for two reasons. First, in the region of BE between E_F and 2 eV, Au has only a weak *sp* conduction band emission and, thus, the emerging features can be assigned to U 5*f* states. Second, α and β are strongly suppressed in He I spectra, which is typical for *f* cross-section behavior,[15] thus, excluding the Au 5*d* origin. The evolution of α and β features within U_xAu_{100-x} series is worth exploring here in detail.

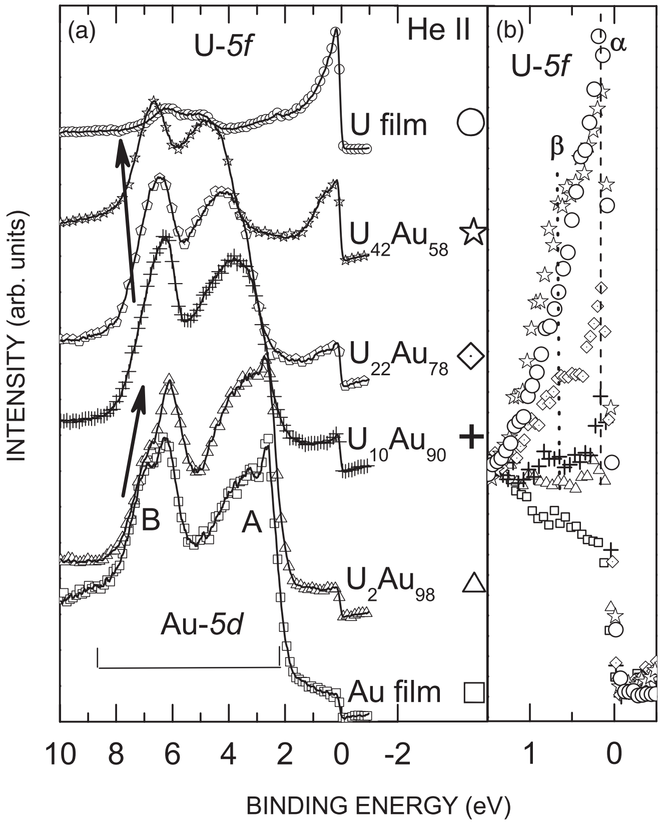

FIG. 1. (a) Selected He II valence spectra of U_xAu_{100-x} films. (b) Superposition of corresponding U 5*f* states in the 0 to 1.5-eV energy domain.

To discuss the evolution of the width of the energy levels with the composition of the films, we choose as a parameter the full width at half maximum (FWHM) of Au 5*d* and U 5*f* peaks (Fig. 2). For the Au 5*d* band, the separate spin-orbit split parts are considered, and for the U 5*f* states, the α and β components are taken (inset Fig. 2). For the Au 5*d* valence band, a continuous narrowing with decreasing Au concentration is observed. The 5*d* bandwidth is related to the number and nature of neighbor atoms. The narrowing shows that the environment of Au atoms is changing under the effect of dilution within the U matrix. The continuity of this process provides a strong argument for a statistical distribution of Au and U atoms without any phase separation. A slope change is observed around 50 at.% and can be due to a percolation effect. Above 80 at.% of U the narrowing proceeds faster. This effect

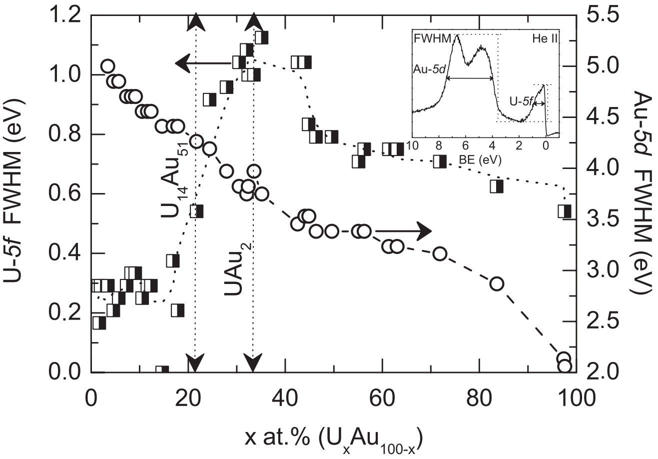

FIG. 2. Full width at half maximum (FWHM) of the Au 5d band and of the U 5f states versus composition of U_xAu_{100-x} films. (Inset) FWHM measurement. The dashed vertical arrows indicate the stable compounds formed in the U-Au system.

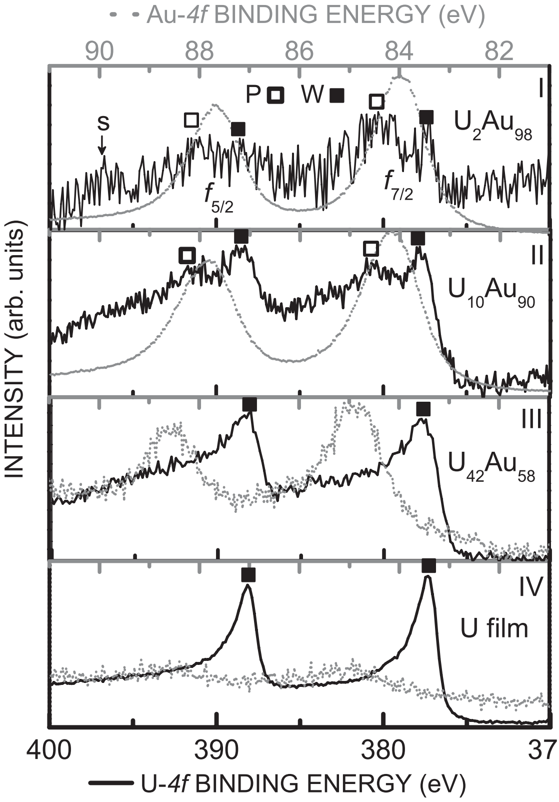

FIG. 3. Selected U 4f and Au 4f core levels of U_xAu_{100-x} films reported for U_2Au_{98} (I), $U_{10}Au_{90}$ (II), $U_{42}Au_{58}$ (III), and U (IV) films.

has been observed for other Au-based compounds[16] and has been related to the composition at which the highest number of unlike neighbor atoms is reached. In other words, it may be explained by an internal charge transfer (5d ↔ 6s) of Au atoms ($5d^{10}6s^1$) isolated in the U matrix. The FWHM of the Au-5d band starts at about 5 eV for pure Au and ends at about 2 eV for Au impurity in a U matrix. The narrowing of the Au 5d band in the presence of U is significantly more pronounced than the narrowing of the Ag 4d band.[3] This is attributed to the fact that Au 5d states participate directly in the alloy bonds.[17] Indeed, among all metals of the periodic table, the ratio of the metal to ionic radius is smallest for Au, suggesting that the 5d shell interacts strongly with the conduction band. Mössbauer isomer shifts also suggested such effects of 5d states, while NMR investigations on Ag alloys showed that the d conduction band is full and d states play little or no role in alloying.[18] For the 5f states (Fig. 2) three distinct regimes are observed according to the FWHM parameter. They are related to the coexistence of features α and β. For $x < 20$–25 at.%, the 5f states are confined to the narrow peak α with a FWHM of about 0.3 eV. This is relatively similar to the FWHM measured for UBe_{13} and UPt_3, which are both heavy fermion compounds and show a sharp peak of 0.15 eV (FWHM) at E_F.[19] Thus, the sharp peak at E_F present in U_xAu_{100-x} for $x < 20$–25 at.% could be associated with a "quasiparticle" state with an enhanced electron mass.[20] This result can also be corroborated with the large value of the low-temperature specific-heat coefficient γ measured for the $U_{14}Au_{51}$ compounds whose composition is equivalent to $U_{21}Au_{79}$ film. The latter displays the two peaks α and β with a higher spectral weight at E_F.

In a second domain of composition (30 at.% $< x <$ 45 at.%), the width increases and passes through a maximum of about 1.1 eV observed for $x = 33$ at.% (corresponding to the stoichiometry of UAu_2 compounds). The broadening of 5f emission is now due to a sum in spectral weight of α and β peaks. With further addition of U ($x >$ 45 at.%), the FWHM decreases slightly, as peak β disappears, and reaches a final value of about 0.6 eV, equal to the width of the narrow peak α measured for pure U. The FWHM of U 5f displays a slope change at about 45–50 at.%. This can be explained by the formation of a pure 5f band with U-U bonding at the detriment of U-Au bonding.

B. Core-level study

The evolution of the Au 4f and U 4f core-level spectra along the U_xAu_{100-x} film series is displayed in Fig. 3. In parallel, Fig. 4 displays the BE shift evolution of Au 4$f_{7/2}$ and the U 4$f_{7/2}$ peaks, relative to the metal, versus the composition of the films ($x = 0$ to 100 at.%). In the following, we, first, focus on U 4f and then on Au 4f core-level spectra.

Along the series ($x = 0$ to 100 at.%), we observed, according to the U 4f peak shapes, four domains of composition, labeled I, II, III, and IV. For each domain we show a representative U 4f and the corresponding Au 4f spectrum [Fig. 3(I) to 3(IV)].

At very low U content, below 5 at.% [Fig. 3(I)], U 4f spectra consist of two spin-orbit split components, 4$f_{7/2}$ and 4$f_{5/2}$, each composed of three peaks, labeled W(■),P (□), and s (sat.). The peaks P and s are separated by about 2.5 and 7.5 eV from the peak W. This three-peak structure is also observed by Hillebrecht *et al.*[9] for highly diluted U (0.85 at.%) in a Au matrix. The intensity of satellite peak s can be correlated to the degree of 5f localization in the matrix; it also provides evidence[21] that the uranium atoms in this domain is in the mixed valence state. Similar U 4f peak shapes [Fig. 3(I)] are also observed in Ce-based compounds[22] and other intermetallic uranium compounds such as UM_2Al_3

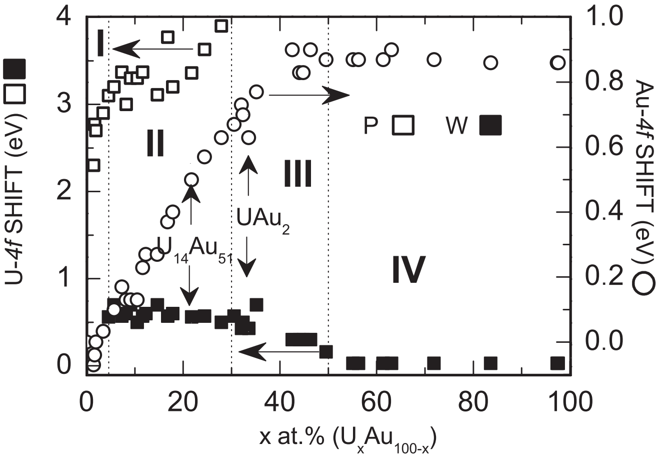

FIG. 4. Binding energy shift of Au $4f_{7/2}$(○) and U $4f_{7/2}$ (well ■ and poorly □ screened peaks) core-level peaks relative to Au and U films, respectively, versus composition x of U_xAu_{100-x} films.

(M = Ni, Pd)[21] and UCu_5M (M = Sn, Al).[23,24] They are a consequence of the interaction between the core hole and the complex outer-shell states[25] and assigned to the $5f^4$ (W), $5f^3$ (P), and $5f^2$ (s) final-state configurations.[21] The low binding energy peak, often referred to as well screened (W), is associated with the final state, where screening of the core hole is done by population of a $5f$ state (f^4). It dominates in systems with well-hybridized $5f$ states. Peak P has been interpreted as the poorly (d-) screened peak and, thus, refers to localized or weakly hybridized $5f$ states. It is the main peak in the Pd-rich domain of U_xPd_{100-x} ($x < 25$ at.%) films.[2] Its energy is also the same as for the oxidized uranium, but the absence of a peak around 1.5 eV below E_F in the valence band spectra [Fig. 1(b)] makes this hypothesis invalid. In domain II, above 5–10 at.% [Fig. 3(II)], the two U $4f_{7/2}$ components (P and W) are observed. The 7.5-eV satellite peak s disappears. Peak P shifts continuously toward higher BE (Fig. 4) and its intensity decreases to the profit of peak W and eventually disappears above the composition of $U_{25}Au_{75}$ film. There is only one experimental spectrum reported on "UAu_3" by Schneider *et al.*[7] showing a single peak for U $4f$. However, the exact composition of the two U-Au phases has been clarified few years after that work. Thus, the real composition of the sample defined by XRD as UAu_3 is doubtful.

In domain III [Fig. 3(III) and Fig. 4], a U $4f$ (W) single peak is observed at 377.6 eV BE. It is strongly asymmetric and has a broad satellite at higher BE [Fig. 3(III), $U_{42}Au_{58}$]. In this domain, the BE and shape of the U $4f$ core level are similar to those observed for UM_2Al_3 compounds where the shape was directly related to the hybridization with ligand states while the contribution from neighboring uranium atoms is negligible.[21] With further addition of U, the screening of the $4f$ hole is made by states of neighboring uranium sites (broad $5f$ band), thus, the U $4f$ peak tends to become sharper and less asymmetric as it appears in U metal film [Fig. 3(IV)]. Along the U_xAu_{100-x} film spectra, the Au $4f$ core-level spectra displays two spin-orbit split components, $4f_{7/2}$ and $4f_{5/2}$, each composed of a single peak [Fig. 3(I) to 3(IV)]. The main effect of U dilution on the latter is the BE shift, whose evolution is described in Fig. 4.

For the pure Au and U films, the Au $4f_{7/2}$ and the U $4f_{7/2}$ lines lie at 84 eV and 377.3 eV BE, in agreement with the literature.[11,26] Below 5 at.% of U, the Au $4f_{7/2}$ core level displays a weak but reproducible shift to lower BE by 0.1 eV. This negative shift may be assigned to a small charge transfer from U to Au, due to their different electronegativity [$\chi_{Au}(2.54) \gg \chi_U$ (1.38) in Pauling scale]. With further addition of U, the Au $4f_{7/2}$ shift gradually moves to higher BE, up to a content of about 45 at.% U. Above this composition the Au $4f_{7/2}$ BE shift saturates at a value of about 0.9 eV. Such a core-level shift to higher BE has been observed for other Au compounds,[27] whereas the corresponding Ag $3d$ shift in U_xAg_{100-x} films[3] was not observed. Again, this may be related to the different electronic structures of Au and Ag bulk. Au has still a partially empty d band, which is involved in bonding by hybridization with the sp conduction band. For this reason, its binding energy changes on dilution with U.[28] At the Au sites, charge redistribution takes place on alloying. The effective charge of d electrons decreases, whereas there is evidence that the $6s$ conduction band is filled, in agreement with the charge compensation model.[16] In this model, the d-band shift to higher BE is an initial-state effect, as it is directly related to the orbital energy. Alternatively, the shift may also be attributed to a final-state screening effect and, again, related to the charge redistribution in the conduction band. With increasing U concentration, the conduction band loses its d character and becomes more s like. Because of the larger screening effect from the d electrons, their loss leads to a higher effective Coulomb potential for the remaining electrons, thereby causing a positive $4f$ BE shift.[16] In addition, the overcompensation of sp charge provides an overall gain of charge to the Au site, in line with electronegativity arguments. The screening tends to be less efficient when U atoms substitute the atoms neighbor of Au, due to a weaker overlapping with Au states.

IV. ELECTRONIC-STRUCTURE CALCULATIONS

To examine the electronic structure of U_xAu_{100-x} theoretically and to make a comparison with experimental data, we investigated the UAu_{15} supercell (see the inset of Fig. 5) which corresponds to 6.25% U concentration. This supercell is chosen to keep the U atom and its 12 nearest Au neighbors separated from the other impurity atoms. The lattice constant of elemental Au is adopted and no geometry relaxation is performed as it is not essential for the close-packed fcc structure.

All calculations are performed making use of the in-house implementation[29,30] of the full-potential linearized augmented plane-wave (FP-LAPW) method. This FP-LAPW version includes all relativistic effects: scalar-relativistic and spin-orbit coupling (SOC). The radii of the atomic muffin-tin (MT) spheres are set to 2.925 a.u. (U) and 2.45 a.u. (Au). The basis set size is characterized by the parameter $R_U \times K_{\max} = 9.7$ and the Brillouin zone is sampled with 343 k points. We have checked that a finer sampling with 729 k points does not modify the results.

First, we apply the conventional local density approximation (LDA) without spin polarization. The calculated f-orbital densities of states (DOS) for the U atom and for the

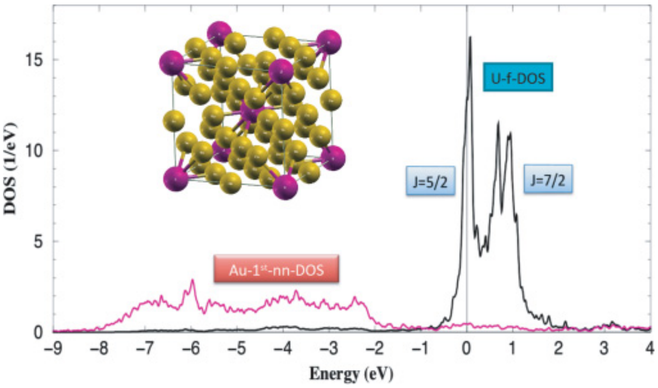

FIG. 5. (Color online) The f-states projected DOS for U impurity in Au calculated with relativistic LDA. First-nearest-neighbor (1st-nn) Au-atom projected DOS is also shown. (Inset) The supercell UAu$_{15}$ model used in calculations.

first-nearest-neighbor Au atoms are shown in Fig. 5. The LDA solution places the U states near the Fermi energy (E_F). They are split by the SOC into $j = 5/2$ and $j = 7/2$ manifolds and are located over the top of the Au-bulk valence band. The U f states projected DOS in Fig. 5 suggests that the hybridization with Au d states is weak. Comparison with valence PE spectra (see Fig. 1) shows that the LDA calculations reproduce the α peak and miss the β satellite.

Next, we apply the spin-polarized LSDA as well as LSDA + U with commonly accepted values for Coulomb $U = 3.0$ eV and exchange $J = 0.585$ eV. We examine different variants of the rotationally invariant LDA + U method:[31] the "fully localized limit" (FLL) as well as the "around mean field" (AMF) version. Both the LSDA and LDA + U methods yield broken-symmetry mean-field solutions with nonzero spin and orbital magnetic moments, M_S and M_L, given in Table I. This is due to the part of the Coulomb interaction treated in the Hartree-Fock-like approximation being transformed into the exchange splitting field. This exchange field is of the order of a few eV [see Fig. 6 (top)]. The LSDA calculations yield f-shell occupation that slightly exceeds its nonmagnetic LDA value of $n_f = 2.7$. When Coulomb U is applied, the $n_f = 2.98$ (FLL) and 3.04 (AMF) becomes close to integer, indicating an increase in f-state localization. Also, the magnitude of the orbital magnetic moment M_L on the U atom increases over its LSDA value due to additional orbital polarization. The spin moment M_S of the U atom decreases in LDA + U (AMF) and increases in LDA + U (FLL) over its LSDA value.

The spin-resolved f-orbital densities of states for U atom calculated from LSDA and LDA + U are shown in Fig. 6 (top). It is seen that while LSDA calculations reproduce the "itinerant" α peak and miss the "localized" β peak, the LDA + U calculations correspond to the "localized" β peak and miss the "itinerant" α peak instead. Our calculations thus demonstrate that none of the approximations employed so far (LDA, LSDA, and LDA + U) are sufficient to accurately describe the U 5f states at the borderline between the localized and itinerant behavior.

TABLE I. Magnetic moments (in μ_B) and 5f occupation n_f of the U impurity in Au host from LSDA a LDA + U calculations.

	M_S	M_L	n_f
LSDA	1.78	−2.63	2.76
LDA + U (FLL)	2.16	−4.66	2.98
LDA + U (AMF)	1.39	−4.15	3.04

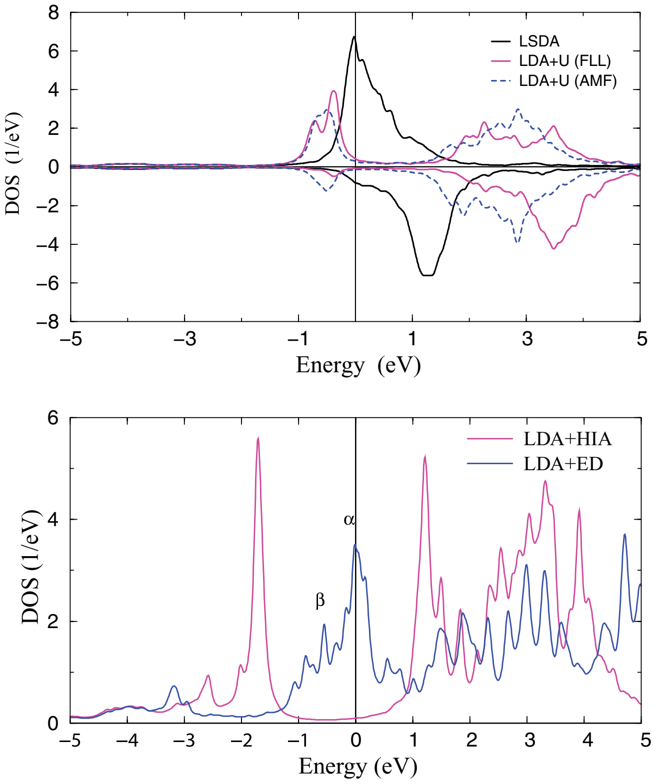

FIG. 6. (Color online) (Top) The spin-resolved f-state projected DOS for U impurity in Au calculated with relativistic LSDA and LDA + U; (bottom) the f-orbital DOS (spectral function) calculated with LDA + ED in comparison with the f-DOS from LDA + HIA calculations. The energy positions of experimental α and β peaks are marked.

The dynamical electron correlations beyond those included in static-mean-field approximations have to be accounted for in order to reproduce the photoemission spectra of hybridized d and f systems.[32] In what follows, we investigate the electronic structure of the UAu$_{15}$ supercell, making use of a new implementation that combines the local density approximation (LDA) with the exact diagonalization (ED)[33] of the single-impurity Anderson model[34] (LDA + ED). The full atomic multiplet structure as well as the hybridization with the conduction band are treated on equal footing with the relativistic band structure discussed above.

The effective multiorbital impurity Hamiltonian can be written as[34]

$$H = \sum_{kmm'\sigma\sigma'} [\epsilon^k]^{\sigma\ \sigma'}_{mm'} b^\dagger_{km\sigma} b_{km'\sigma'} + \sum_{m\sigma} \epsilon_f f^\dagger_{m\sigma} f_{m\sigma}$$
$$+ \sum_{mm'\sigma\sigma'} [\xi \mathbf{l}\cdot\mathbf{s} + \Delta_{\mathrm{CF}}]^{\sigma\ \sigma'}_{mm'} f^\dagger_{m\sigma} f_{m'\sigma'}$$

$$+\sum_{kmm'\sigma\sigma'}\left([V^k]^{\sigma\ \sigma'}_{mm'}f^\dagger_{m\sigma}b_{km'\sigma'}+\text{h.c.}\right)$$
$$+\frac{1}{2}\sum_{mm'm''m'''\sigma\sigma'}U_{mm'm''m'''}f^\dagger_{m\sigma}f^\dagger_{m'\sigma'}f_{m'''\sigma'}f_{m''\sigma}, \quad (1)$$

where $f^\dagger_{m\sigma}$ creates an electron in the f shell and $b^\dagger_{m\sigma}$ creates an electron in the "bath" that consists of those host-band states that hybridize with the impurity f shell. The impurity-level position ϵ_f and the bath energies ϵ^k are measured from the chemical potential μ. The parameters ξ and Δ_{CF} specify the strength of the spin-orbit coupling and the size of the crystal field at the impurity. The parameter matrices V^k describe the hybridization between the f states and the bath at the energies ϵ^k.

The calculations were carried out assuming a paramagnetic state. The Slater integrals were chosen as $F_0 = 3.0$ eV, $F_2 = 7.09$ eV, $F_4 = 4.6$ eV, and $F_6 = 3.36$ eV, that is, the same as in the LDA + U calculations. The single-particle parameters ξ and Δ_{CF} were determined from LDA calculations as $\xi = 0.28$ meV and $\Delta_{\mathrm{CF}} = 0$. The first and fourth terms in Eq. (1) are assumed to be diagonal in the $\{j, j_z\}$ representation. To construct a minimal model of the impurity-bath hybridization we then need to specify one bath state (six orbitals) with $\epsilon^{j=5/2}_{k=1}$ and $V^{j=5/2}_{k=1}$ and another bath state (eight orbitals) with $\epsilon^{j=7/2}_{k=1}$ and $V^{j=7/2}_{k=1}$. These four bath-related parameters are determined from the assumption that LDA represents the noninteracting model for the U impurity in Au host. In other words, the LDA results are associated with the solution of Eq. (1) without the last Coulomb-interaction term. Assuming that only the hybridization which occurs in the vicinity of E_F is essential for the problem at hand, we obtain $V^{j=5/2,7/2}_{k=1}$ by averaging the relation $\sum_k |V^j_k|^2\delta(\epsilon^j_k-\epsilon) = \Delta^j(\epsilon)$,[35] where $\Delta^j = \frac{1}{\pi N_j}\,\mathrm{Im}\,\mathrm{Tr}_j[G^{-1}_{\mathrm{LDA}}(\epsilon+i0)]$ for $j = 5/2$ and $7/2$ manifolds, over the energy region $E_F \pm 0.5$ eV. Next, we adjust $\epsilon^{5/2,7/2}_{k=1}$ to approximately reproduce the LDA values for the $5f$-state occupations $n^{5/2}_f$ and $n^{7/2}_f$.

After the parameters of the discrete impurity model are set, the band Lanczos method[36,37] is utilized to determine the lowest-lying eigenstates of the many-body Hamiltonian and to calculate the one-particle Green's function in the subspace of the f orbitals $[G_{\mathrm{imp}}(z)]^{\sigma\ \sigma'}_{mm'}$ at low temperature ($k_BT = 2$ meV). The impurity self-energy $[\Sigma(z)]^{\sigma\ \sigma'}_{mm'}$ is then straightforwardly obtained from the inverse of the Green's function matrix $[G_{\mathrm{imp}}(z)]^{\sigma\ \sigma'}_{mm'}$.

Once the self-energy is known, the local Green's function $G(z)$ for the electrons in the solid is calculated as

$$[G(z)]^{-1}_{\gamma_1\gamma_2} = [G_{\mathrm{LDA}}(z)]^{-1}_{\gamma_1\gamma_2} - \Delta\epsilon\,\delta_{\gamma_1\gamma_2} - [\Sigma(z)]_{\gamma_1\gamma_2}, \quad (2)$$

where $\Delta\epsilon$ accounts for the difference between the impurity and the lattice chemical potentials and $G_{\mathrm{LDA}}(z)$ is the LDA Green's function,

$$[G_{\mathrm{LDA}}(z)]_{\gamma_1\gamma_2} = \frac{1}{V_{\mathrm{BZ}}}\int_{\mathrm{BZ}} d^3k\,[z+\mu-H_{\mathrm{LDA}}(\mathbf{k})]^{-1}_{\gamma_1\gamma_2}. \quad (3)$$

For the charge-density self-consistency, we employ the so-called local density matrix approximation (LDMA).[38] In the LDMA, the occupation matrix

$$n_{\gamma_1\gamma_2} = -\frac{1}{\pi}\,\mathrm{Im}\int_{-\infty}^{E_{\mathrm{F}}} dz\,[G(z)]_{\gamma_1\gamma_2} \quad (4)$$

is evaluated with the aid of the local Green's function $G(z)$ from Eq. (2). The matrix $n_{\gamma_1\gamma_2}$ is then used to construct an effective LDA + U potential V_U, which is inserted into Kohn-Sham-like equations,

$$[-\nabla^2 + V_{\mathrm{LDA}}(\mathbf{r}) + V_U + \xi(\mathbf{l}\cdot\mathbf{s})]\Phi^b_{\mathbf{k}}(\mathbf{r}) = \epsilon^b_{\mathbf{k}}\Phi^b_{\mathbf{k}}(\mathbf{r}). \quad (5)$$

These equations are iteratively solved until self-consistency over the charge density is reached. In each iteration, a new Green's function $G_{\mathrm{LDA}}(z)$ and a new value of the f-shell occupation are obtained from the solution of Eq. (5). Subsequently, a new self-energy $\Sigma(z)$ corresponding to the updated f-shell occupation is constructed. Finally, the next iteration is started by inserting the new $G_{\mathrm{LDA}}(z)$ and $\Sigma(z)$ into Eq. (2). After the iterations are completed, the imaginary part of the local Green's function $G(z)$ provides a means to estimate the valence-band photoemission (PE) spectra.

The ground state of the cluster formed by the f shell and the bath, Eq. (1), includes, on average, $\langle n_f\rangle = 2.70$ electrons in the f shell and $\langle n_{\mathrm{bath}}\rangle = 6.30$ electrons distributed among the bath states. It is not a singlet and the U atom can be viewed as being in a mixed valence state. The spin $S = 1.28$, orbital $L = 5.59$, and total $J = 4.34$ moments are calculated for the f shell from the expectation values $\langle\hat{X}^2\rangle = X(X+1)$, $X = S, L, J$. The individual components of the moments vanish, $\langle\hat{S}_z\rangle = \langle\hat{L}_z\rangle = 0$.

The resulting f-orbital DOS (spectral function) is shown in Fig. 6 (bottom). It is seen that LDA + ED reproduces both the α peak at E_F and the β satellite at ≈0.5 eV below E_F. Overall, the agreement with experimental PE spectra is very reasonable.

Finally, we compare LDA + ED with a simpler method, LDA + Hubbard-I (LDA + HIA),[38] where only the atomic multiplet effects are included and no hybridization with the conduction band is taken into account, that is, the first and fourth terms are omitted from Eq. (1). The corresponding LDA + HIA DOS consists of two "Hubbard bands" away from E_F, in disagreement with experimental PE spectra in Fig. 1. These results show that hybridization is essential for explaining the PE in U-based systems, starting from a single U impurity.

V. CONCLUSION

In this study, we have investigated the effect of dilution on $5f$ states in a Au matrix. It is concluded that the $5f$ states, even at high dilution, are hybridized with the conduction band. Schneider *et al.*[7] interpreted the XPS spectrum of bulk "$\mathrm{UAu_3}$" (close to $\mathrm{U_{14}Au_{51}}$) in terms of itinerant $5f$ electrons, whereas Petit *et al.*[8] assigned it to a localized $5f^2$ configuration, similarly to $\mathrm{UPd_3}$. Our study shows that, for the U-Au system, the $5f$ states never become completely localized, in contrast to $\mathrm{U}_x\mathrm{Pd}_{100-x}$ series.[2] The electronic configuration of U in Au matrix differs from a $5f^2$ configuration present in the Pd matrix. Throughout the series of $\mathrm{U}_x\mathrm{Au}_{100-x}$ thin films we observed the evolution from a (5f, ligand states) ($x < 25$ at.%) hybrid band to a pure 5f band ($x > 50$ at.%). The transition goes through the competition between these two interactions as shown by the broad band of 5f peaks. The presence of the main U 5f peak just at E_F is consistent with the observed high electronic specific-heat coefficient of the $U_{14}Au_{51}$ bulk compound. The complex satellite structure observed for highly diluted uranium in the core-level spectra suggests that the uranium atoms have a mixed final-state configuration, as in the case of other uranium heavy fermions systems. The LDA + ED electronic structure calculations explain well the main photoemission features and illustrate the essential role of hybridization in the U-based systems.

ACKNOWLEDGMENTS

We acknowledge R. Caciuffo and J.-C. Griveau for fruitful discussions. The support from Czech Republic Grants No. GACR P204/10/0330, No. GAAV IAA100100912, and No. AV0Z10100520 is acknowledged.

---

*rachel.eloirdi@ec.europa.eu

[1] R. Eloirdi, T. Gouder, F. Wastin, J. Rebizant, and F. Huber (private communication).

[2] R. Eloirdi, T. Gouder, F. Wastin, and J. Rebizant, J. Alloys Compd. **372**, 10 (2004).

[3] R. Eloirdi, T. Gouder, P. A. Korzhavyi, F. Wastin, and J. Rebizant, J. Alloys Compd. **386**, 70 (2005).

[4] A. Palenzona and S. Cirafici, J. Less-Common Met. **143**, 167 (1988).

[5] A. Dommann and F. Hulliger, J. Less-Common Met. **141**, 261 (1988).

[6] H. R. Ott, E. Felder, A. Schilling, A. Dommann, and A. F. Hulliger, Solid State Commun. **71**, 549 (1989).

[7] W.-D. Schneider and C. Laubschat, Phys. Rev. B **23**, 997 (1981).

[8] L. Petit, A. Svane, W. M. Temmerman, and Z. Szotek, Phys. Rev. Lett. **88**, 216403 (2002).

[9] F. U. Hillebrecht, H. J. Trodahl, V. Sechovsky, and B. T. Thole, Z. Phys. B **77**, 373 (1989).

[10] F. U. Hillebrecht, V. Sechovsky, and B. T. Thole, J. Magn. Magn. Mater. **76&77**, 353 (1988).

[11] P. H. Citrin, G. K. Wertheim, and Y. Baer, Phys. Rev. B **27**, 3160 (1983).

[12] H. Piao and N. S. McIntyre, J. Electron Spectrosc. Relat. Phenom. **119**, 29 (2001).

[13] H. Piao, N. S. McIntyre, G. Beamson, M.-L. Abel, and J. F. Watts, J. Electron Spectrosc. Relat. Phenom. **125**, 35 (2002).

[14] A. D. McClean and R. S. McClean, At. Data Nucl. Data Tables **26**, 197 (1981).

[15] J. J. Yeh and I. Lindau, At. Data Nucl. Data Tables **32**, 1 (1985).

[16] M. Kuhn and T. K. Sham, Phys. Rev. B **49**, 1647 (1994).

[17] R. E. Watson, J. Hudis, and M. Perlman, Phys. Rev. B **4**, 4139 (1971).

[18] T. J. Rowland, Phys. Rev. **119**, 900 (1960).

[19] A. J. Arko *et al.*, J. Less-Common Met. **133**, 87 (1987).

[20] A. J. Arko, C. G. Olson, D. M. Wieliczka, Z. Fisk, and J. L. Smith, Phys. Rev. Lett. **53**, 2050 (1984).

[21] S.-I. Fujimori, Y. Saito, N. Sato, T. Komatsubara, S. Suzuki, S. Sato, and T. Ishii, Solid State Commun. **105**, 185 (1998).

[22] J. W. Allen, S. J. Oh, O. Gunnarsson, K. Schonhammer, M. B. Maple, M. S. Torikachvili, and I. Landau, Adv. Phys. **35**, 275 (1986).

[23] G. Chelkowska, J. A. Morkowski, A. Szajek, and R. Troc, J. Phys. Condens. Matter **14**, 3199 (2002).

[24] G. Chelkowska, J. A. Morkowski, A. Szajek, and R. Troc, Phys. Rev. B **64**, 075119 (2001).

[25] W.-D. Schneider and C. Laubschat, Phys. Rev. Lett. **46**, 1023 (1981).

[26] J. F. Moulder, W. F. Stickle, P. E. Sobol, and K. D. Bomben, *Handbook of X-Ray Photoelectron Spectroscopy*, edited by J. Chastain (Perkin-Elmer, Norwalk, CT, 1992).

[27] S. B. DiCenzo, S. D. Berry, and E. H. Hartford, Phys. Rev. B **38**, 8465 (1988).

[28] P. H. Citrin, G. K. Wertheim, and Y. Baer, Phys. Rev. Lett. **41**, 1425 (1978).

[29] A. B. Shick, D. L. Novikov, and A. J. Freeman, Phys. Rev. B **56**, R14259 (1997).

[30] A. B. Shick and W. E. Pickett, Phys. Rev. Lett. **86**, 300 (2001).

[31] A. I. Liechtenstein, V. I. Anisimov, and J. Zaanen, Phys. Rev. B **52**, R5467 (1995).

[32] A. Georges, G. Kotliar, W. Krauth, and M. Rozenberg, Rev. Mod. Phys. **68**, 13 (1996).

[33] J. Kolorenč, unpublished (2010); see also M. Cheng and H.-H. Tu, Phys. Rev. B **84**, 094503 (2011).

[34] A. C. Hewson, *The Kondo Problem to Heavy Fermions* (Cambridge University Press, Cambridge, 1993).

[35] O. Gunnarsson, O. K. Andersen, O. Jepsen, and J. Zaanen, J. Phys. Rev. B **39**, 1708 (1989).

[36] A. Ruhe, Math. Comput. **33**, 680 (1979).

[37] H.-D. Meyer and S. Pal, J. Chem. Phys. **91**, 6195 (1989).

[38] A. B. Shick, J. Kolorenč, A. I. Lichtenstein, and L. Havela, J. Phys. Rev. B **80**, 085106 (2009).